



Reactive Magnetron Sputtering of ZrO_2/Al_2O_3 Coatings: Alumina Content and Structure Stability

I. Zukerman^{1,2,*}, R.L. Boxman² and A. Raveh³

¹NRC-Negev, P.O. Box 9001, Beer-Sheva 84190, Israel

²Electrical Discharge and Plasma Laboratory, Faculty of Engineering, Tel-Aviv University, Tel-Aviv, Israel

³Advanced Coatings Center, Rotem Industries Ltd., Mishor Yamin, D.N. Arava 86800, Israel

Abstract: Ternary zirconia-alumina coatings with different compositional ratios, ranging from pure zirconia to 50% alumina content, were deposited by reactive sputtering from two targets, Zr and Al, in argon-oxygen mixtures. The coating composition was controlled by the Zr/Al target power ratio provided by two pulsed-DC power supplies. The coatings were ~1 μm thick and they were deposited on floating potential substrates at a temperature of $650\pm 3\text{K}$.

XRD indicated that the pure zirconia coatings possessed a monoclinic structure with a grain size of 35–40 nm. Adding alumina to the zirconia coating stabilized the cubic zirconia phase and decreased the grain size to 10–15 nm. The alumina phase in the coatings remained amorphous. The hardness of the nanocomposite structure increased from 11.6 ± 0.5 GPa to 16.1 ± 0.5 GPa for an alumina content of 17%. At higher alumina concentrations, the zirconia phase became amorphous and the hardness decreased to 10–11 GPa.

Structure stability of the zirconia-alumina coatings was studied by measuring the coating structure and hardness after annealing at temperatures up to 1173 K. Pure zirconia (*m*- ZrO_2) coatings had low structure stability; the hardness reached a maximum value of 18 ± 1 GPa after annealing at a temperature of 773–873K; however, at higher annealing temperatures the hardness decreased, reaching a minimum value of 12.3 ± 0.6 GPa after annealing at 1173K. The hardness of the nanocomposite ZrO_2/Al_2O_3 coating with various compositions increased with annealing temperature. The hardness of a coating with an alumina content of 17% reached a high value of 19.2 ± 0.5 GPa after annealing at 1073–1173 K. Measurements of post annealing XRD analyses indicated that the stabilization of the coating structure with *c*- ZrO_2/a - Al_2O_3 phases is the reason for the higher structure stability. From the analyses of phase stability and hardness before and after annealing, we conclude that adding alumina to the zirconia phase promotes the formation of nanocomposite *c*- ZrO_2/a - Al_2O_3 coatings with a markedly higher stability than single-phase *m*- ZrO_2 .

Highlights:

1. ZrO_2/Al_2O_3 nanocomposite coatings were deposited by co-sputtering from Zr and Al targets.
2. Adding alumina to the zirconia coating stabilized the cubic zirconia phase.
3. ZrO_2 -17% Al_2O_3 coatings had a grain size of 10–15 nm and a hardness of 16.1 ± 0.5 GPa.
4. ZrO_2/Al_2O_3 coatings maintained a high hardness after annealing at 1173K with a high value of 19 GPa for alumina content of 17%.
5. The ZrO_2/Al_2O_3 nanocomposite coatings were crack-free after annealing at 1173K.

Received on 20-08-2015
Accepted on 26-08-2015
Published on 14-09-2015

Keywords: Stabilized Zirconia, Thin coatings, Magnetron sputtering, Hardness, thermal treatments.

DOI: <http://dx.doi.org/10.6000/2369-3355.2015.02.02.4>

1. INTRODUCTION

Zirconia coatings offer a variety of applications due to their high ionic conductivity, high corrosion resistance, low thermal

conductivity, high refractive index, high fracture toughness and good mechanical stability [1]. Zirconia generally exhibits three possible phases, monoclinic (*m*- ZrO_2) phase, stable at room temperature till 1443K, and two high temperature phases, tetragonal (*t*- ZrO_2) and cubic (*c*- ZrO_2) [2]. It is well known that the addition of another element, like yttria [3] or alumina [4], stabilized the zirconia coatings to its high

*NRC-Negev, P.O. Box 9001, Beer-Sheva 84190, Israel; Tel: +972-506238856; Fax: +972-86569015; E-mail: idozukerman@gmail.com

temperature phase. The addition of second element was also used to increase the coating resistance to cracking [5]. The ZrO_2/Al_2O_3 system has almost no mutual solubility [6] and therefore, it offers a possibility to be formed as hard nanocomposites with high thermal stability [7].

ZrO_2/Al_2O_3 coatings were deposited by various physical vapor deposition techniques as nanolaminate [8-10] or nanocomposite [5, 11-14] systems. Most of the early studies focused on t- ZrO_2 phase stabilization using alternating layers of the alumina phase. For example, in nanolaminate ZrO_2/Al_2O_3 coatings, formation of the t- ZrO_2 phase is controlled by the modulation thickness of the Al_2O_3 and ZrO_2 layers [8, 15] (the Al_2O_3 layers are amorphous). The nanolaminated coatings showed excellent phase stability after annealing at $T_a=973K$ for 56 hours [15], however, at $T_a=1273K$, the ZrO_2 transformed to monoclinic phase due to grain growth [16]. Further study showed that t- ZrO_2 phase can be stabilized up to annealing temperature of $T_a=1773K$ by amorphous SiO_2 phase [17].

Structure of nanocomposite Al-Zr-O coatings deposited using magnetron sputtering and ZrO_2 - rich composition, exhibit a t- $ZrO_2/a-Al_2O_3$ (a=amorphous) or c- $ZrO_2/a-Al_2O_3$ structure, in contrast to pure m- ZrO_2 coatings [11, 13]. With high Al_2O_3 content, the coatings become amorphous. The ZrO_2 phase (tetragonal or cubic) and the Al_2O_3 content limiting crystallization of the ZrO_2 phase are controlled by the substrate temperature and by the deposition method [13]. Among the parameters that most affect the ZrO_2 crystallization are the power mode (pulsed-DC or radio-frequency) and target material (metallic or oxide). Coatings

with Al_2O_3 - rich composition, high hardness (~ 30 GPa) and $\gamma-Al_2O_3/a-ZrO_2$ structure can also be deposited by reactive sputtering [11]. Such high hardness was obtained when the ZrO_2 content was below 7 at.%, while an increased content of the minor phase (ZrO_2) amorphized the coating [11]. These results, on both ends of the Al_2O_3/ZrO_2 system (ZrO_2 - rich and Al_2O_3 - rich coatings), suggest a strong tendency for segregation [11, 13].

The influence of deposition parameters and of ZrO_2/Al_2O_3 composition on the coatings phase formation is fairly understood. However, the structure stability of nanocomposite ZrO_2/Al_2O_3 coatings was not studied. In this respect, understanding ZrO_2/Al_2O_3 coating behavior is essential for high-temperature applications. The objective of this study was to determine the influence of the alumina content before and after thermal treatments on the coatings structure and hardness. This paper reports on the deposition of ZrO_2/Al_2O_3 coatings using a dual pulsed-DC reactive magnetron sputtering technique. The first part reports the influence of the Al_2O_3 phase content on the structure and properties of the as-deposited coatings. The second part reports on the structure stability of the coatings, studied by post annealing hardness and x-ray diffraction analysis.

2. EXPERIMENTAL DETAILS

The ZrO_2/Al_2O_3 coatings were prepared in a dual DC-reactive magnetron sputter deposition reactor illustrated in Figure 1. The reactor was equipped with two magnetron sputtering units in open magnetic field configuration, one mounted with a 51 mm aluminum target (99.999% purity) and the second

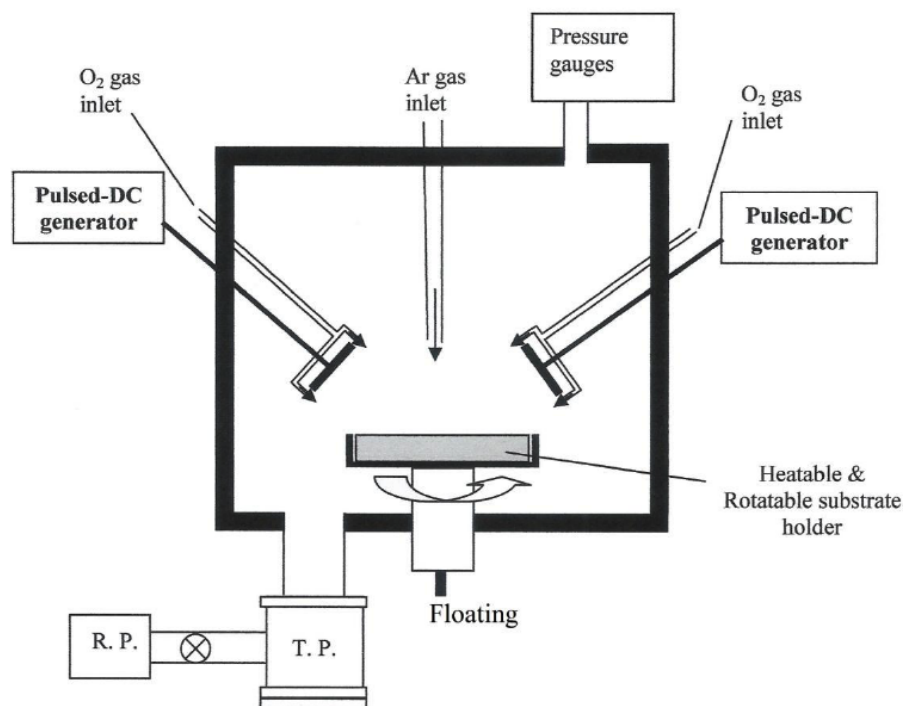


Figure 1: Schematic diagram of the reactive magnetron sputtering system. T.P.- turbomolecular pump, R.P. - Rotary pump.

one with a 51 mm zirconium target (99.9% purity). Each sputtering unit was powered by a pulsed direct current (pulsed-DC) generator and has its own oxygen inlet. The substrate, 300 μm thick (001) crystalline silicon wafers, 51 mm in diameter, were cleaned in acetone and placed on a heatable and rotatable substrate holder located 70 mm from each target.

Before deposition, the reactor was pumped down using turbomolecular and rotary pumps to a base pressure of 1×10^{-4} Pa, following which a mixture of argon (99.999% purity) and oxygen (99.999% purity) was introduced. The oxygen flow rate was 20 vol.% of the total flow of 100 sccm. The total pressure was $P=1.9$ Pa, with $P_{\text{Ar}}=1.4$ Pa and $P_{\text{O}_2}=0.5$ Pa. All depositions were performed in the power controlled mode, with synchronized DC-pulses between the Zr and Al target, pulse repetition rate of 350 kHz and a duty cycle of 55%. ZrO_2 coatings were deposited with a Zr target power of 200 W. The $\text{ZrO}_2/\text{Al}_2\text{O}_3$ coating composition was varied by changing the power to the aluminum target (20-200 W), while keeping the zirconium target power at a constant value of 200 W. The substrate temperature during all depositions was kept at 650K using a halogen lamp heater. The substrate holder was kept at the floating potential while rotating at 1 RPM. The deposition time was 120 minutes for all coatings.

After deposition, the structure of the coatings was analyzed by X-ray diffraction (XRD) using a Rigaku D Max 2000 diffractometer with Cu-K α radiation. The grain size was calculated from the XRD spectra using the Williamson-Hall method [18]. The microstructure was examined using scanning electron microscopy, (HRSEM, JOEL JSM-7400D). The coating composition was studied with X-ray photoelectron spectroscopy (XPS) using an ESCALAB 250 spectrometer with an Al X-ray source and a monochromator. The hardness, H , of the layers was measured using a diamond Vickers indenter with a load of 5 mN. Residual stress, σ , was analyzed by the curvature method, using the Stoney equation [19].

The structure stability of the coatings was studied by annealing the coatings at temperatures of $T_a=773, 973, 1073$ and 1173 K for one hour in vacuum (10^{-4} Pa). After annealing, the coatings were analyzed by XRD, and corresponding H values were assessed.

3. RESULTS

3.1. Structure and Composition

All coatings deposited in this study had a thickness of 1.0 ± 0.1 μm , which gives a deposition rate of 0.5 ± 0.1 $\mu\text{m}/\text{h}$, a value typical for sputter deposition of $\text{ZrO}_2/\text{Al}_2\text{O}_3$ coatings in the oxide deposition mode [5]. XPS measurement found only Al, Zr and O in the coatings, following surface cleaning (etched to ~ 10 nm depth). Figure 2 shows the atomic concentration (Figure 2a) and the Al/(Zr+Al) concentration ratio (Figure 2b) as function of the targets power ratio. The aluminum content increased, linearly, with the increase of the Al/Zr targets power ratio (Figure 2b). Oxygen concentrations in the ZrO_2 coatings were over-stoichiometric (the solid line in Figure 2a represent the calculated oxygen concentration, expected from the Al and Zr content, for stoichiometric oxides), while the oxygen concentration of $\text{ZrO}_2/\text{Al}_2\text{O}_3$ coatings was lower than expected from their Zr and Al ratios. This means that the ZrO_2 phase in the $\text{ZrO}_2/\text{Al}_2\text{O}_3$ coatings should be under-stoichiometric, as the formation enthalpy of Al_2O_3 ($\Delta H_{\text{Al}_2\text{O}_3}=-1678\text{KJ}/\text{mol}$) is lower compared to ZrO_2 ($\Delta H_{\text{ZrO}_2}=-1101\text{KJ}/\text{mol}$) [5].

High resolution XPS, as well as the XRD analysis (Figure 3) found no evidence to metallic phases in the coatings. It is known that ZrO_2 and Al_2O_3 have almost no miscibility [6, 7]. Thus, we assumed that there is no Zr-Al-O compound in the coatings. Based on these, it is reasonable to state that the aluminum and zirconium contents in the coatings represent the Al_2O_3 and ZrO_2 concentrations, respectively. Henceforth, we will present the coating composition as the aluminum

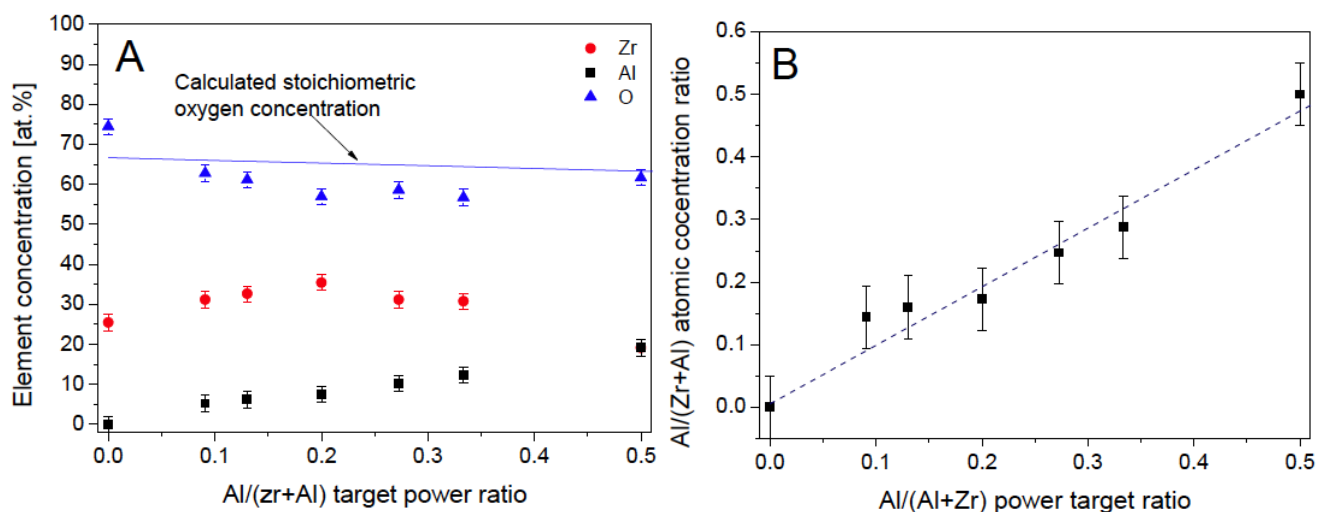


Figure 2: Coating elements content (A) and Al/(Zr+Al) element content ratio (B) as a function of the Zr/(al+Zr) target power ratio. The solid line represents the calculated oxygen concentration, expected from the Al and Zr content, for stoichiometric oxides.

content of the total amount of aluminum and zirconium (for example, Zr14Al state for coatings with 14 at.% alumina content).

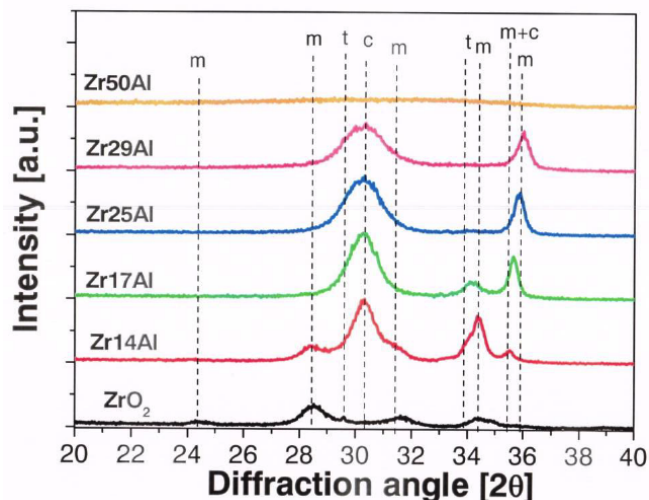


Figure 3: XRD patterns with different coating compositions. The dashed lines represent the major diffraction peaks of the ZrO_2 phases. c- cubic, t- tetragonal, m- monoclinic. The sample numbers represent the Al_2O_3 content in the coating. Deposition parameters: Zr target power- 200 W, gas flow- 100 sccm (Ar + 20% O_2), substrate temperature- 650 K, deposition time- 2 hours.

Figure 3 shows the coating XRD patterns for different coating compositions. The ZrO_2 coating was mostly monoclinic, with some minor t- ZrO_2 phase (see the peak at 29.7°) and a grain size of 40 ± 5 nm, typical of ZrO_2 coatings deposited at floating or zero substrate bias [20]. In contrast, ZrO_2/Al_2O_3 coatings were composed mainly of c- ZrO_2 . It is difficult to determine the exact amount of the ZrO_2 phases in each coating due to the large number of possible peaks and the overlap between them. Even so, the peak at 28.2° is characteristic of m- ZrO_2 (-111), and the peak at 30.5° is characteristic to either c- ZrO_2 (111) or t- ZrO_2 (111). The nonexistence of the main t- ZrO_2 (101) at 29.8° indicates that the 30.5° peak originates from the c- ZrO_2 phase. As no Al_2O_3 peaks were identified in the XRD, we assume that the ZrO_2 grains are surrounded by a- Al_2O_3 [5, 9, 13].

The structure of sample Zr14Al was a mixture of c- ZrO_2 and m- ZrO_2 phases. The presence of t- ZrO_2 in this coating cannot be ruled out, as the diffraction peak at 34.3° could be either t- ZrO_2 (111) or m- ZrO_2 (020). With a further increase in the alumina content (sample Zr17Al), the main m- ZrO_2 peak (-111, at 28.2°) disappeared, proving that the peak at 34.3° was belong to t- ZrO_2 (111). Thus, the coating structure was a mixture of c- ZrO_2 and t- ZrO_2 phases. For samples Zr17Al to Zr29Al, peak broadening was observed with the increase in the alumina content from 17% to 29%, respectively. The peak broadening was observed together with the decrease of the t- ZrO_2 peak, which did not appear in sample Zr25Al that contained 25% alumina. Both c- $ZrO_2/a-Al_2O_3$ [13] and t- $ZrO_2/a-Al_2O_3$ [5, 9, 11] structures were reported in the literature.

The peak at 35.8° appearing in sample Zr14Al and then shifting towards 36.0° (sample Zr29Al) can be attributed to m- ZrO_2 . However, we attribute the $\sim 36^\circ$ peak position to the present of sub-stoichiometric ZrO_{2-x} or $Zr_xAl_yO_z$ phases. This identification is due to the absent of the main m- ZrO_2 phase and because of the shifting of this peak to higher diffraction angles as the Al_2O_3 content increases. During simultaneous deposition of Zr and Al in an oxygen environment, the formation of Al_2O_3 is favorable compared to ZrO_2 as a result of higher negative enthalpy [5]. Therefore, if the oxygen flux to the coating surface is insufficient to form both Al_2O_3 and ZrO_2 , it appears that under-stoichiometric ZrO_x phase is preferentially formed. The XPS results (Figure 2) showed that the composition of the ZrO_2/Al_2O_3 coatings exhibits a sub-stoichiometric ratio. The increase in the Al_2O_3 content enhanced the under-stoichiometry of the ZrO_2 and decreased the lattice parameter of ZrO_{2-x} (which shifts the diffraction peak towards higher angles). The substitution of Al atoms in the ZrO_2 matrix and the formation of $Zr_xAl_yO_z$ cannot be ruled out as the deposition temperature (650K) is lower than the temperature predicted for complete segregations of the ZrO_2 and Al_2O_3 phases (823-1023K [7]). The formation of $Zr_xAl_yO_z$ phase could be an alternative explanation to the presence of the peak at $35.8-36.0^\circ$.

Figure 4 shows SEM cross-section photographs of ZrO_2 (Figure 4a) and ZrO_2/Al_2O_3 (Figure 4b-d) coatings. The ZrO_2 coating had a typical columnar structure. The coating microstructure of all ZrO_2/Al_2O_3 coatings up to 25at.% Al_2O_3 content, had a similar structure to the ZrO_2 coating (e.g., see Figure 4b). At higher Al_2O_3 content, the structure was featureless (characteristic of amorphous coatings), at the substrate interface in Figure 4c, and throughout the coatings for sample Zr50Al (Figure 4d).

Figure 5a shows the hardness as a function of coating composition. With increasing alumina content, H increased from 11.6 ± 0.4 GPa for ZrO_2 coatings to 16.1 ± 0.9 GPa for sample Zr17Al. Then, H decreased to 11.3 ± 0.5 GPa with a further increase in the alumina content. Similar decrease in hardness was observed by Klostermann *et al.* [11]. The grain size (Figure 5b) was analyzed by the XRD peak broadening of the ZrO_2 phase. The grain size decreased consistently with the increase in alumina content, from 40 ± 5 nm for ZrO_2 coatings, through $18-19\pm 5$ nm for Zr14Al and Zr17Al coating and to $10-11\pm 5$ nm for Zr25Al and Zr29Al coatings.

Generally, the residual stress observed in our study was relatively low. Single-phase ZrO_2 coating had compressive stress, $\sigma = -50$ MPa, while all ZrO_2/Al_2O_3 coatings had tensile stress increasing values with Al_2O_3 content up to $\sigma = +270$ MPa for sample Zr29Al. The low stress is characteristic to coatings deposited with zero substrate bias [21, 22] or at relatively high working pressure (~ 3 Pa in this work) [20].

3.2. Structure Stability

Figure 6 shows XPS depth profiles of ZrO_2 and Zr17Al coatings after annealing at 1073K for 1 hour. It was found

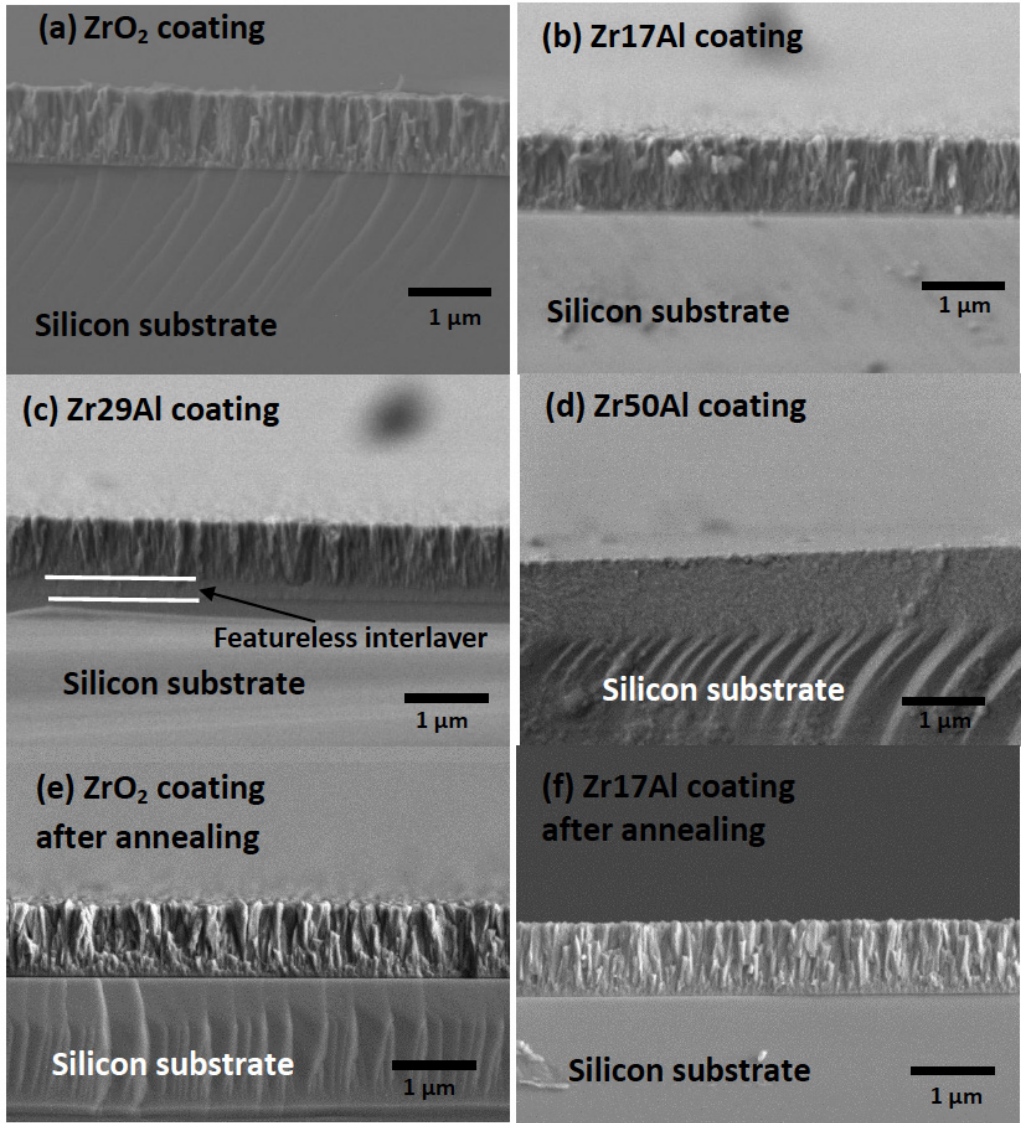


Figure 4: Cross section SEM images of ZrO_2 and ZrO_2/Al_2O_3 coatings. (a) ZrO_2 , (b) Zr25Al, (c) Zr29Al, (d) Zr50Al, (e) ZrO_2 after annealing at 1073 K, (f) Zr17Al after annealing at 1073 K. The sample numbers represent the Al_2O_3 content in the coating. Deposition parameters: Zr target power- 200 W, gas flow- 100 sccm (Ar + 20% O_2), substrate temperature- 650 K, deposition time- 2 hours.

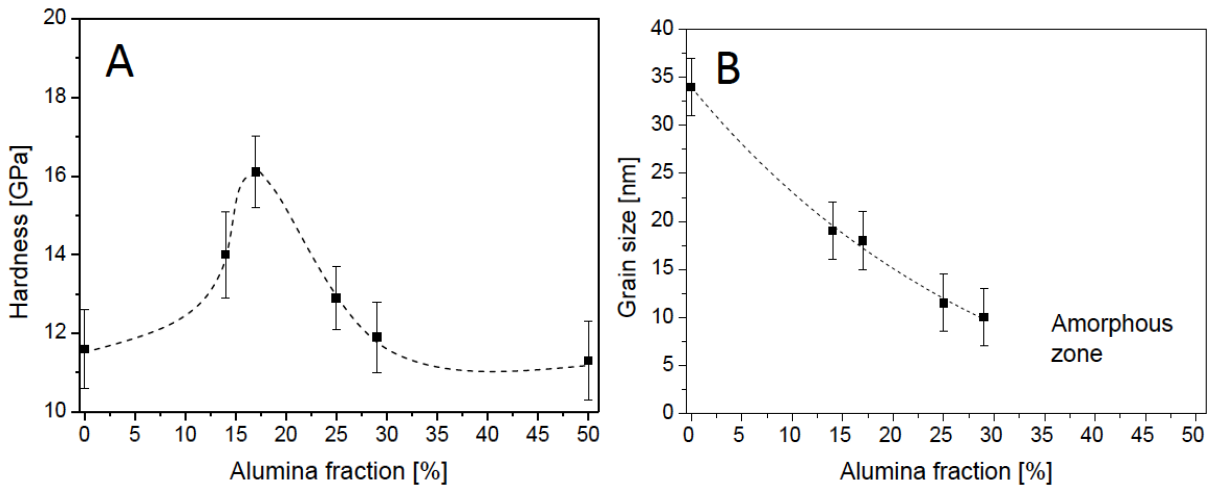


Figure 5: Coatings hardness (A) and grain size (B) as a function of the coatings composition. Vickers indenter, 5 mN load. Deposition parameters: Zr target power- 200 W, gas flow- 100 sccm (Ar + 20% O_2), substrate temperature- 650 K, deposition time- 2 hours.

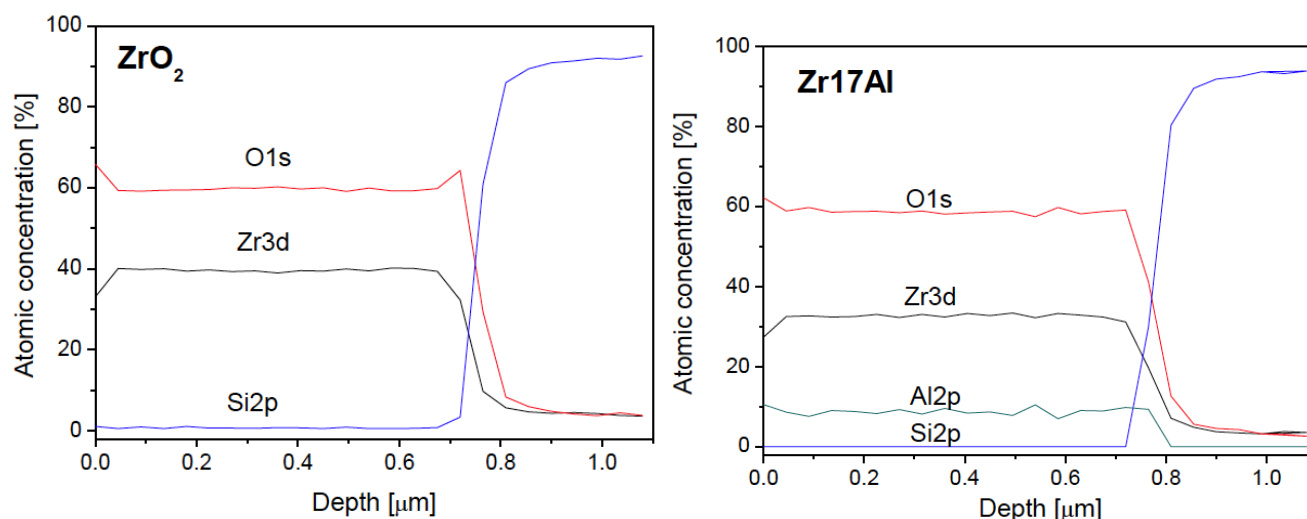


Figure 6: XPS depth profile of ZrO_2 and Zr17Al coatings after annealing.

that the thermal treatment did not change the coating homogeneity or the coating composition. Also, no silicon diffusion from the substrate to the coatings was observed. Figure 7 shows the post-annealing hardness for different coating compositions. The hardness of ZrO_2 (black squares) increased to 17.9 ± 0.8 GPa after annealing at $T_a = 773$ – 873 K. However, with a further increase in T_a , H decreased to 12.3 ± 1.2 GPa ($T_a = 1173$ K). The post annealing hardness of the composite ZrO_2/Al_2O_3 coatings was higher than the single phase ZrO_2 coatings. Furthermore, the hardness of the various composite ZrO_2/Al_2O_3 coatings was higher after annealing than that measured prior to annealing. A maximum hardness of 19.2 ± 0.5 GPa was found for sample Zr17Al after annealing at 1073–1173 K.

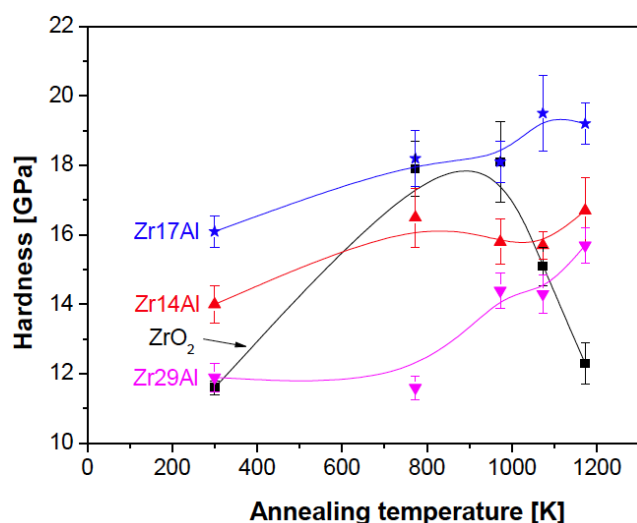


Figure 7: Post-annealing hardness of ZrO_2 and various ZrO_2/Al_2O_3 coatings (Vickers indenter, 5 mN load). The sample numbers represent the Al_2O_3 content in the coating.

ZrO_2/Al_2O_3 coatings were crack-free after annealing at $T_a = 1173$ K, compared to ZrO_2 coatings which were completely cracked after annealing at $T_a \geq 1073$ K. Nevertheless, in

ZrO_2/Al_2O_3 coatings with Al_2O_3 content of ≥ 25 at.%, cracks appeared during the indentation test, clearly indicating on coating brittleness [23].

Figure 8 shows the XRD patterns of samples Zr14Al, Zr17Al and Zr29Al, as well as the ZrO_2 coating, before and after annealing at 1173 K. The structure of the Zr14Al sample after annealing (Figure 8a) changed to a c- ZrO_2/a - Al_2O_3 structure, while the m- and t-phases disappeared. Moreover, the main c- ZrO_2 peak shifted, after annealing, to its undistorted position (30.5°). The XRD pattern of the Zr17Al sample (Figure 8b) showed the same shift of the c- ZrO_2 peak to its undistorted position, while the t- ZrO_2 peak (at 34.3°) disappeared, and the peak at 35.8° increased and shifted to a larger diffraction angle. This peak is not related to m- ZrO_2 because neither the main (-111) peak at 28.7° nor any other m- ZrO_2 peaks were present in the XRD pattern. The XRD pattern of the Zr29Al sample (Figure 8c) revealed no major changes from the annealing. Again, the c- ZrO_2 peak shifted to its undistorted position (30.5°). In contrast to the ZrO_2/Al_2O_3 coatings, the structure of the ZrO_2 coating (Figure 8d) changed from mainly m- ZrO_2 to a mixture of m-, t- and c- ZrO_2 . SEM analysis of the ZrO_2 and Zr17Al coatings after annealing (Figure 4e-f) showed columnar growth compared to the as-deposited coatings (Figure 4a-b). This growth was more pronounced in the ZrO_2 coating which showed some voids between columns. These results are consistent with the peak increase in the XRD results (Figure 8) which is more pronounced in the ZrO_2 coatings.

4. DISCUSSION

The addition of Al_2O_3 to the ZrO_2 coating changed the coating structure, and stabilized the zirconia component into c- ZrO_2 or t- ZrO_2 phases. This effect was already reported for both nanolayered ZrO_2/Al_2O_3 coatings [8] and nanocomposite ZrO_2/Al_2O_3 coatings [11, 13] deposited at low temperatures. Trinh *et al.* [13] attributed the formation of the cubic structure to oxygen under-stoichiometry, elastic restraint from the

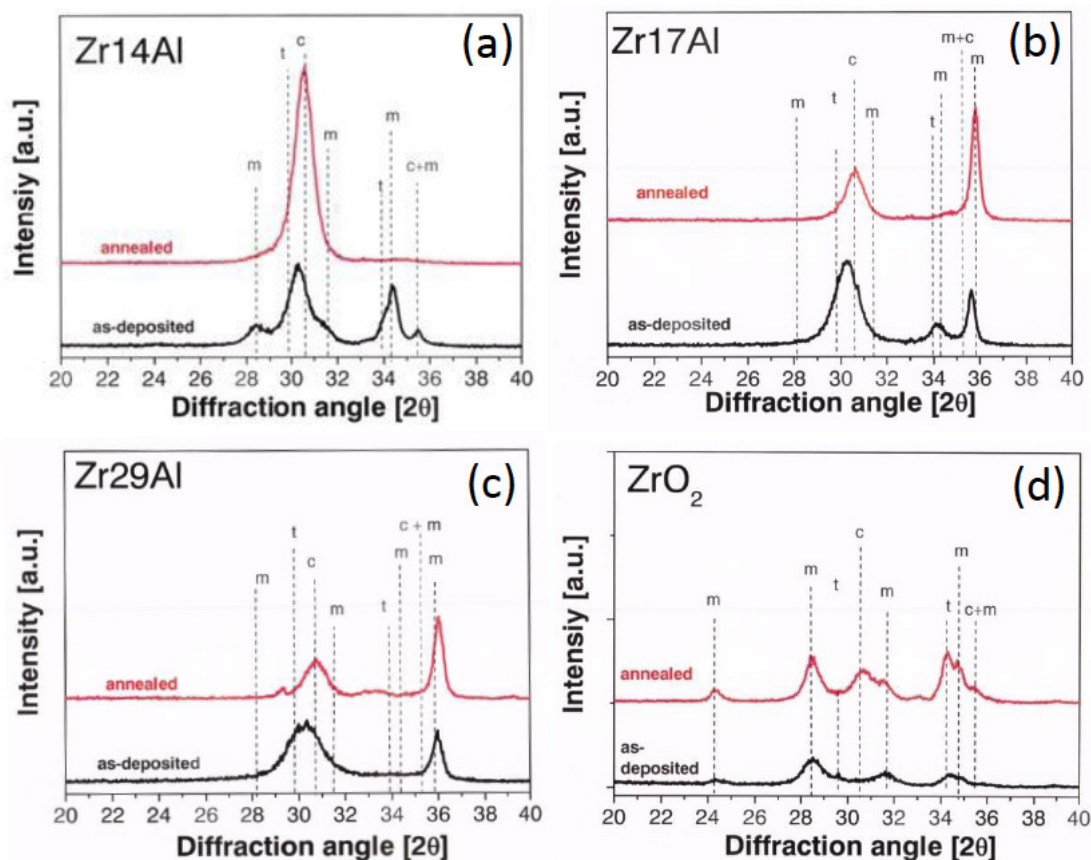


Figure 8: XRD patterns of Zr14Al (a), Zr17Al (b), Zr29Al (c) and ZrO₂ (d) samples, before and after annealing at 1073 K. The sample numbers represent the Al₂O₃ content in the coating.

alumina phase, or a combination of both. During simultaneous deposition of Zr and Al in an oxygen environment, the formation of Al₂O₃ is more favorable than ZrO₂, due to higher negative enthalpy [5]. Therefore, we may conclude that if the oxygen flux to the coating surface is insufficient to form both Al₂O₃ and ZrO₂, an under-stoichiometric ZrO_x phase will preferentially formed.

The addition of Al₂O₃ also increased H by 50% up to 16 GPa (sample Zr17Al) and refined the ZrO₂ grains size. However, the results in this study (Figure 5) show that the increase in hardness cannot be explained only by grain refinement, as coating with grain size of 10-11 μm (Zr25Al, Zr29Al coatings) had lower hardness compared sample Zr17Al with grain size of $\sim 20 \mu\text{m}$. This implies that the ZrO₂/Al₂O₃ coating system has an optimal Al₂O₃ content with ordering of ZrO₂ grains and amorphous Al₂O₃ phase [7].

The ZrO₂ coating showed low structure stability. Although the hardness of the ZrO₂ coatings initially increased with $T_a=773$ -883K, it then steeply decreased at higher T_a . The thermal treatment improved the crystallinity of the ZrO₂ coating (Figure 8d) which is probably the reason for the increase in hardness at low T_a . However, the recovery at $T_a \geq 1083$ K resulted in grain growth (Figures 4e and 8d) and decrease in hardness.

The ZrO₂/Al₂O₃ coatings showed higher structural stability than the ZrO₂ coatings, up to 1173K. Although the Al₂O₃ content in the coatings varied between 14-29%, the post-annealing hardness after $T_a=1173$ K was higher than the as-deposited hardness (Figure 7). Similar to the ZrO₂ coating, the increase in hardness after thermal treatment is mainly due to improved crystallinity. This is observed after annealing in the XRD patterns by the shift of the c-ZrO₂ peak towards its theoretical position, while other ZrO₂ phases disappeared (seen most clearly for the Zr14Al sample, Figure 8a). These results indicated that the c-ZrO₂/a-Al₂O₃ is stable structure of the coatings, at least up to 1173K.

The nano-composite ZrO₂/Al₂O₃ coatings were crack-free after the thermal cycle to $T_a=1173$ K. However, coatings with high Al₂O₃ contents (25-50at.%) showed radial cracking after the Vickers indentation test, indicating on coating brittleness [23]. The high resistance to cracking of ZrO₂/Al₂O₃ coatings with low Al₂O₃ content (<25at.%) is similar to the results presented by Musil *et al.* [5, 24]. Musil [24] explained the high resistance to cracking by high $H/E^* \geq 0.1$, high elastic recovery ($W_e > 60\%$), compressive stress (in the present study the ZrO₂/Al₂O₃ coatings had low tensile stress) and dense, void-free microstructure. The higher brittleness of the high Al₂O₃ contents coatings is not fully understood yet and it may be due to lower H/E^* ratio compared to the low Al₂O₃ contents coatings [5].

The ZrO₂ coatings were completely cracked after annealing to $T_a \geq 1073\text{K}$. The cracking of the ZrO₂ coatings can be explained by the large difference between the linear expansion coefficients of m-ZrO₂ coatings ($\alpha = 10.6 \cdot 10^{-6}/\text{K}$ [25]) and the Si substrate ($\alpha = 2.6 \cdot 10^{-6}/\text{K}$ [26]) and the low $H/E^* = 0.05$ [8] of ZrO₂ coatings. The cracking cannot be explained by m-ZrO₂ to t-ZrO₂ transformation, as $T_a = 1173\text{K}$ well below the transformation temperature (1443K). The fact that the c-ZrO₂/a-Al₂O₃ coatings were crack-free after annealing (although, c-ZrO₂ phase has higher linear expansion coefficient, $\alpha = 13.5 \cdot 10^{-6}/\text{K}$ [25], compared to m-ZrO₂), shows the high stability of the c-ZrO₂/a-Al₂O₃ coatings.

The self-hardening and structural changes of the coatings during annealing indicated that the as-deposited coatings were in a meta-stable state, due to insufficient deposition temperature. With annealing, the coatings completely segregated into the c-ZrO₂/a-Al₂O₃ structure. Although the high-temperature behavior of the nanocomposite ZrO₂/Al₂O₃ coatings is still not fully understood, the results presented in this study show the clear potential of Al₂O₃ in improving the structure stability of the ZrO₂/Al₂O₃. This finding is despite that the coating was deposited at temperature lower the temperature predicted for complete segregations of the ZrO₂ and Al₂O₃ phases [7].

5. CONCLUSIONS

As-deposited ZrO₂/Al₂O₃ coating structure was only partially stabilized as c-ZrO₂/a-Al₂O₃ due to the low deposition temperature (650K). However, thermal treatments stabilized the coating structure up to 1173 K. It was concluded from this study that the addition of moderate amounts of Al₂O₃ to ZrO₂ coatings stabilized the ZrO₂ in the cubic phase (in contrast to monoclinic for pure ZrO₂ coatings). At Al₂O₃ contents above 30%, the coatings became amorphous. Moreover, the addition of 17% Al₂O₃ content to the coatings increased the hardness from ~11 GPa, for pure ZrO₂, to ~16 GPa. Nanocomposite ZrO₂/Al₂O₃ coatings with Al₂O₃ content $\leq 29\%$ had higher structure stability than single-phase ZrO₂ coatings. The improved structure stability resulted in high hardness of up to 19 GPa, after annealing at 1173K of ZrO₂-17% Al₂O₃ coatings. Similar occurrence was also observed in coatings with higher or lower Al₂O₃ contents which reached hardness of ~16 GPa after annealing at 1173K. Therefore, the high post-annealing hardness is due to stabilization of the coating structure of c-ZrO₂/a-Al₂O₃ after annealing.

ACKNOWLEDGEMENTS

The authors are grateful to Mr. Tomer Even-Hen for XRD measurements and to Mr. Avi Ben-Shabat for expert technical assistance.

REFERENCES

[1] Chang JT, Yeh CH, He JL, Chen KC, Matthews A, Leyland A. Deposition of yttria-stabilized zirconia films using arc ion plating. Surf Coat Technol 2005; 200: 1401-6. <http://dx.doi.org/10.1016/j.surfcoat.2005.08.091>

[2] Green DJ, Hannink RHJ, Swain MV. Transformation Toughening of Ceramics, CRC, Boca Raton FL 1989.

[3] Lange FF. Transformation toughening, Part 3: Experimental observations in the ZrO₂-Y₂O₃ system. J Mater Sci 1982; 17: 240-6. <http://dx.doi.org/10.1007/BF00809059>

[4] Lange FF. Transformation toughening, Part 4: Fabrication, fracture toughness and strength of Al₂O₃-ZrO₂ composites. J Mater Sci 1982; 17: 247-54. <http://dx.doi.org/10.1007/BF00809060>

[5] Musil J, Sklenka J, Cerstvy R, Suzuki T, Mori T, Takahashi M. The effect of addition of Al in ZrO₂ thin film on its resistance to cracking. Surf Coat Technol 2012; 207: 355-60. <http://dx.doi.org/10.1016/j.surfcoat.2012.07.017>

[6] Jerebtsov DA, Mikhailov GG, Sverdina SV. phase diagram of the system: ZrO₂-Al₂O₃. Ceram Int 2000; 26: 821-3. [http://dx.doi.org/10.1016/S0272-8842\(00\)00023-7](http://dx.doi.org/10.1016/S0272-8842(00)00023-7)

[7] Sheng SH, Zhang RF, Veprek S. Study of spinodal decomposition and formation of nc-Al₂O₃/ZrO₂ nanocomposites by combined ab initio density functional theory and thermodynamic modeling, Acta Materialia 2011; 59: 3498-509. <http://dx.doi.org/10.1016/j.actamat.2011.02.023>

[8] Barshilia HC, Deepthi B, Rajam KS. Stabilization of tetragonal and cubic phases of ZrO₂ in pulsed sputter deposited ZrO₂/Al₂O₃ and ZrO₂/Y₂O₃ nanolayered thin films. J Appl Phys 2008; 104: 113532. <http://dx.doi.org/10.1063/1.3040720>

[9] Teixeira V, Monteiro A, Duarte J, Portinha A. Deposition of composite and nanolaminate ceramic coatings by sputtering. Vacuum 2002; 67: 477-83. [http://dx.doi.org/10.1016/S0042-207X\(02\)00235-X](http://dx.doi.org/10.1016/S0042-207X(02)00235-X)

[10] Kim SK, Le VV, Boxman RL, Zhitomirsky VN, Lee JY. Cathodic arc plasma deposition of nano-multilayered Zr-O/Al-O thin films. Surf Coat Technol 2010; 204: 1697-701. <http://dx.doi.org/10.1016/j.surfcoat.2009.10.037>

[11] Klostermann H, Bocher B, Fietzke F, Modes T, Zywitzki O. Nanocomposite oxide and nitride hard coatings produced by pulse magnetron sputtering. Surf Coat Technol 2005; 200: 760-4. <http://dx.doi.org/10.1016/j.surfcoat.2005.02.120>

[12] Qadri SB, Gilmore CM, Quinn C, Skelton EF, Gossett CR. Structural stability of ZrO₂-Al₂O₃ thin films deposited by magnetron sputtering. J Vac Sci Technol 1989; A7: 1220-4. <http://dx.doi.org/10.1116/1.576258>

[13] Trinh DH, Kubart T, Nyberg T, Ottosson M, Hultman L, Hogberg H. Direct current magnetron sputtering deposition of nanocomposite alumina-zirconia thin films. Thin Solid Films 2008; 516: 8352-8. <http://dx.doi.org/10.1016/j.tsf.2008.04.040>

[14] Zukerman I, Zhitomirsky VN, Beit-Yakov G, Boxman RL, Raveh A, Kim SK. Vacuum arc deposition of Al₂O₃-ZrO₂ coatings: arc behavior and coating characteristics. J Mater Sci 2010; 45: 6379-88. <http://dx.doi.org/10.1007/s10853-010-4734-7>

[15] Aita CR, Scanlan CM, Gajdardziska-Josifovska M. Sputter deposited zirconia-alumina nanolaminate coatings. JOM 1994; 46: 40-2. <http://dx.doi.org/10.1007/BF03222607>

[16] Andrichsky M, Cunha I, Alpuim P. Thermal stability of zirconia/alumina thin coatings produced by magnetron sputtering. Surf Coat Technol 1997; 94-95: 144-8. [http://dx.doi.org/10.1016/S0257-8972\(97\)00492-1](http://dx.doi.org/10.1016/S0257-8972(97)00492-1)

[17] Musil J, Satava V, Zeman P, Cerstvy R. Protective Zr-containing SiO₂ coatings resistant to thermal cycling in air up to 1400 °C. Surf Coat Technol 2009; 203: 1502-7. <http://dx.doi.org/10.1016/j.surfcoat.2008.11.026>

[18] Williamson GK, Hall WH. X-ray line broadening from filed Al and W. Acta Metall 1953; 1: 22-31. [http://dx.doi.org/10.1016/0001-6160\(53\)90006-6](http://dx.doi.org/10.1016/0001-6160(53)90006-6)

[19] Ohring M (2002) The Materials Science of Thin Films 2nd Ed., Academic Press Inc., San Diego, pp. 547-588.

[20] Koski K, Holsa J, Juliet P. Properties of zirconium oxide thin films deposited by pulsed reactive magnetron sputtering. Surf Coat Technol 1999; 120-121: 303-12. [http://dx.doi.org/10.1016/S0257-8972\(99\)00501-0](http://dx.doi.org/10.1016/S0257-8972(99)00501-0)

[21] Rickerby DC, Burnett PJ. Correlation of process and system parameters with structure and physically vapor deposited hard coatings. Thin Solid Films 1988; 157: 195-222. [http://dx.doi.org/10.1016/0040-6090\(88\)90004-1](http://dx.doi.org/10.1016/0040-6090(88)90004-1)

[22] Koski K, Holsa J, Juliet P. Deposition of aluminum oxide thin films by reactive magnetron sputtering. Thin Solid Films 1999; 339: 240-8. [http://dx.doi.org/10.1016/S0040-6090\(98\)01232-2](http://dx.doi.org/10.1016/S0040-6090(98)01232-2)

- [23] Giannakopoulos AE, Larsson PL, Vestergaard R. Analysis of Vickers indentation. *Int J Solid Structures* 1994; 31: 2679-708.
[http://dx.doi.org/10.1016/0020-7683\(94\)90225-9](http://dx.doi.org/10.1016/0020-7683(94)90225-9)
- [24] Musil J. Flexible hard nanocomposite coatings. *RSC Advances* 2015; 5:60482-95.
<http://dx.doi.org/10.1039/C5RA09586G>
- [25] ASM Handbook, Vol. 20, Materials selection and design, 1997
- [26] Watanabe H, Yamada N, Okaji M. Linear thermal expansion coefficient of silicon from 293 to 1000K. *Int J Thermophys* 2004; 25: 221-36.
<http://dx.doi.org/10.1023/B:IJOT.0000022336.83719.43>